Quantitative detection of multi-frequency disturbance signal by ϕ-OTDR system

To cite this article: Ya-Jun Wang *et al* 2023 *Meas. Sci. Technol.* **34** 034002

View the article online for updates and enhancements.

Quantitative detection of multi-frequency disturbance signal by φ-OTDR system

Ya-Jun Wang[1], **Bin Liu**[1,*]📷, **Juan Liu**[1], **Jinhui Yuan**[3,4,*], **Yanjun Fu**[1], **Xing-Dao He**[1] **and Qiang Wu**[1,2,*]📷

[1] Key Laboratory of Opto-Electronic Information Science and Technology of Jiangxi Province, Nanchang Hangkong University, Nanchang 330063, People's Republic of China
[2] Optical Communications Research Group. Faculty of Engineering and Environment, Northumbria University, Newcastle Upon Tyne NE1 8ST, United Kingdom
[3] Research Center for Convergence Networks and Ubiquitous Services, University of Science & Technology Beijing, Beijing 100083, People's Republic of China
[4] State Key Laboratory of Information Photonics and Optical Communications, Beijing University of Posts and Telecommunications, Beijing 100876, People's Republic of China

E-mail: liubin@nchu.edu.cn, yuanjinhui81@bupt.edu.cn and qiang.wu@northumbria.ac.uk

Abstract
Recently, the combination of pattern recognition technology and distributed fiber sensing systems has become increasingly common, so whether the disturbance signal can be well recovered has become increasingly important. To verify the recovery and linear response of a distributed fiber optic sensing system to multi-frequency disturbance signals, a heterodyne coherent detection system for phase-sensitive optical time-domain reflectometry is developed. The output beat signal is extracted using the digital in-phase/quadrature demodulation algorithm. The signal can be precisely located on a 7 km length range, and the disturbance signal can be restored well through the phase information. Not only the superposition signal composed of the same signal but also that composed of different kinds of signals can be successfully restored. A fast Fourier transform algorithm is used to obtain the frequency information of the superimposed signal. Combined with the use of a finite impulse response filter, the superposed signal is decomposed according to its frequency components, which perfectly restores the two signals before they are superimposed. In addition, their amplitude is highly linear with the driving voltage of the piezoelectric transducer. The system can fully retain the details of each frequency component in the recovery of multi-frequency disturbance signals. More importantly, in field experiments, the disturbance behavior is well recovered, which has broad prospects in the application of perimeter security.

Keywords: φ-OTDR, multifrequency disturbance, quantitative detection, I/Q demodulation

(Some figures may appear in colour only in the online journal)

---

* Authors to whom any correspondence should be addressed.

1. Introduction

Recently, distributed optical fiber sensing (DOFS) has gradually entered people's field of vision. Phase-sensitive optical time-domain reflectometry (φ-OTDR) exploits the self-coherence phenomenon of back Rayleigh scattering in optical fibers to obtain phase and amplitude information of perturbation events [1]. It also has many excellent properties, such as long detection range, high sensitivity, and the capability to detect multi-point perturbation [2, 3]. Therefore it can be used very well in many ways, for example, structural monitoring of buildings [4], rail transit [5], pipeline protection [6], and perimeter security [7].

Nowadays, in order to improve DOFS technology performance in practical applications, many people focus on the improvement of system performance. For instance, Chen *et al* proposed a Pearson correlation coefficient fusion method to improve the signal-to-noise ratio (SNR) [8]. A highly sensitive intrusion detection system structure combining distributed Raman amplification and heterodyne detection was proposed by Peng *et al*; the detection length of this system reached 131.5 km [9]. In addition, some research directions are focused on improving spatial resolution, such as edge detection [10] or optical frequency-swept pulse [11]. Others focus on extracting phase information from external disturbances. This is because, in the application of a DOFS system in perimeter security, it is obviously far from enough to locate the disturbance in practical applications. Recently, with the increasing popularity of pattern recognition technology, the application of the technology to perimeter security has become a research hot topic [12].

Early φ-OTDR systems detected external perturbation events only by extracting the amplitude information of the Rayleigh backward scattering (RBS) light. Due to the random interference effect that occurs in the process of light transmission, the received backscattered light undergoes a large amplitude change, which is signal fading [13, 14]. Due to the fading of the signal and the existence of random noise, it is difficult to recover the external disturbance accurately via the amplitude. Therefore, using phase information to recover the external disturbance signal has emerged as a solution. Phase recovery technology mainly includes interference technology and in-phase/quadrature (I/Q) demodulation technology. Typical interferometer techniques include the 3×3 optical coupler [15, 16] and the unbalanced Michelson interferometer combined with a phase-generating carrier (PGC) [17, 18]. At the same time, various improved systems have emerged. For example, Wang *et al* proposed a scheme based on a homodyne detection system combined with a digital I/Q demodulation algorithm [19], which mainly introduces a 90° optical mixer into the system to generate a pair of signals with a 90° phase difference. An IQ demodulation algorithm is used for phase extraction. Although this reduces the amount of calculation, the 90° optical mixer part has problems such as extra loss and non-orthogonal amplitude and phase due to the limitations of the production process. In order to reduce the introduction of additional modulators, Yu *et al* proposed

an improved PGC demodulation algorithm and applied it to the φ-OTDR system [20]. It not only reduces the amount of data computation but also extracts phase information from the disturbance signal. However, it lacks validation of the linearity of the system response. Fang *et al* proposed a Michelson interferometric fiber optic acoustic sensor based on a large area gold diaphragm [21], which adopted the elliptic fitting differential cross multiplication demodulation algorithm with high SNR and good linear response. However, the system structure is relatively complex. Liu *et al* introduced phase-shifted double-pulse probe technology to realize the quantitative demodulation of low-frequency disturbance signals, which cannot detect multi-frequency disturbance signals [22]. Therefore, this paper proposes to use the heterodyne coherent detection [23] system with a relatively simple structure to develop a new multi-frequency perturbation scheme, and further verify it with the perturbation of the actual scene.

In this paper, the recovery and quantitative detection of the external multi-frequency interference signal are verified over a φ-OTDR system. Superposition signals composed of both the same and different types of signals with different frequencies can be successfully recognized and restored. More importantly, the superposed signal is decomposed according to its frequency components, perfectly restoring the two signals before they are superimposed; in addition, their amplitude is highly linear with the driving voltage of the piezoelectric transducer (PZT). At the same time, rapid field validation tests are performed.

2. Experimental setup and principle

Figures 1(a) and (b) show the system block diagram and a photo of experimental setup, respectively. First, a continuous line of light is emitted by a narrow linewidth laser (NLL, MCNLFL-1550, MC Fiber Optics Co., Ltd.), and the linewidth of this continuous light is about 1 kHz with a wavelength of 1550.12 nm. A 10:90 optical coupler (OC1, 1550-DWC-1*2, Huashun Communications Equipment Co., Ltd.) splits this light into two signals. This 10% light can be used as a reference signal, and then an acoustic optical modulator (AOM, G-1550-80-L-D-T-AA-A-T-L, Conquer Optoelectronic Technology Co., Ltd) modulates this 90% light into a pulsed light and introduces a frequency shift of 80 MHz with a pulse width of 100 ns. Its corresponding spatial resolution is about 10 m. After the pulse is amplified by an erbium-doped fiber amplifier (EDFA, KY-EDFA-PL-10-D-FA, Keyang Optoelectronic Technology Co., Ltd.), it enters the fiber under test (FUT, G652D) through a circulator (CIR, QIHAXUKA-15-P-2-1-1, QIHAXUKA Technology Co., Ltd.). An isolator (ISO, ISO-S-1550-900L-1-FA) prevents Fresnel reflection peaks from appearing in the back Rayleigh scattering curve. The returning RBS light and reference light are coupled in a 50:50 optical coupler (OC2, 1550-DWC-2*2, Huashun Communications Equipment Co., Ltd.), and detected by a balanced photodetector (BPD, KY-BPRM-BW-I-FA, Keyang Optoelectronic Technology Co., Ltd.). The acquisition rate of the data
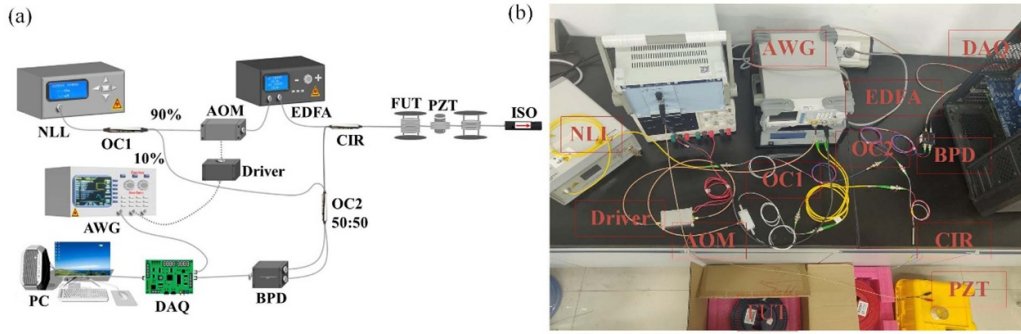
Figure 1. (a) System block diagram and (b) experimental setup. BPD: balanced photodetector; NLL: narrow linewidth laser; CIR: circulator; EDFA: erbium-doped fiber amplifier; AWG: arbitrary wave generator; AOM: acoustic optical modulator; PC: personal computer; PZT: piezoelectric transducer; ISO: isolator; DAQ: data acquisition card; FUT: fiber under test; OC: optical coupler.

acquisition card (DAQ, QT1144VG-2, Queentest Technology Co., Ltd.) is 250 MSa s^{-1}, and it transmits the collected electrical signals to a personal computer for processing and display. An arbitrary waveform generator (AWG, DG1022Z, RIGOL Technologies Co., Ltd.) can provide a drive signal to the AOM and a synchronous trigger signal for the DAQ. The FUT is a common single-mode fiber in which approximately 10 m of fiber is tightly wound around a cylindrical PZT (OD50-ID45-TH50, Φ50 mm $\times$ φ45 mm $\times$ 50 mm, Core Tomorrow Science & Technology Co., Ltd.). The signal from the function generator is first transmitted to a signal amplifier to amplify the signal to 15 times (the voltage values listed in this paper are those after amplification), and then to the PZT as the driving signal to generate vibrations in the sensing fiber.

In this system, the reference is $E_{\mathrm{L}}(t)\exp\{i[\omega_{c}t+\varphi_{0}(t)]\}$. Scattering light can be expressed as $E_{\mathrm{R}}(t)\exp\{i[\omega_{c}t+\Delta\omega t+\varphi(t)]\}$. $E_{\mathrm{R}}(t)$ and $E_{\mathrm{L}}(t)$ are the amplitudes of the RBS and reference, respectively. $\Delta\omega$ is the frequency shift generated by the AOM. ω_{c} is the center frequency of the NLL. $\varphi_{0}(t)$ is the phase value of the reference light. $\varphi(t)$ is the phase value of the scattered light. The BPD collects beat signals generated by the Rayleigh backscattering and reference, and the output power is expressed by the following formula:

$$P_{\mathrm{BPD}} \propto E_{\mathrm{R}}(t)E_{\mathrm{L}}(t)\cos\left[\Delta\omega t+\varphi(t)-\varphi_{0}(t)\right]. \quad (1)$$

Assuming that the acquisition rate of the DAQ card is f_s, the digital signal collected by DAQ can be represented by the following formula:

$$S(n) \propto E_{\mathrm{L}}(n)E_{\mathrm{R}}(n)\cos\left[\Delta\omega_{n}n+\varphi_{s}(n)\right], n=1,2,3,\ldots,N. \quad (2)$$

The digital angular frequency in the formula is $\Delta\omega_n = 2\pi\Delta f/f_s$, phase $\varphi_s(n) = \varphi(n)-\varphi_0(n)$, where n and N are the number and total number of sampling points, respectively. DAQ sends the collected digital signal $S(n)$ into the computer for I/Q demodulation. Figure 2 shows the collected beat signal $S(n)$, and the I/Q demodulation algorithm flow is shown in figure 3.

Digital signal $S(n)$ is respectively multiplied by sine and cosine digital signals with the same digital angular frequency
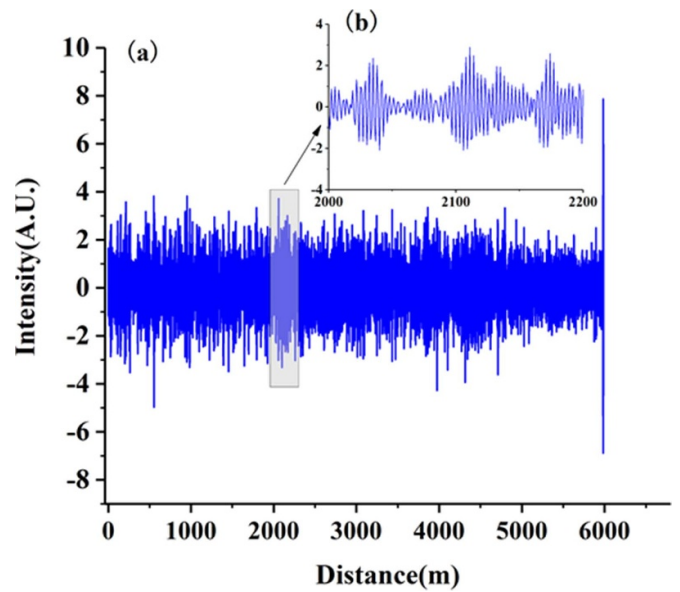
Figure 2. (a) Collected beat signal $S(n)$, (b) magnified view of local area.

$\Delta\omega_n$, and then the output of I and Q obtained through the digital low pass filter can be expressed as:

$$I \propto E_{\mathrm{L}}(n)E_{\mathrm{R}}(n)\cos\varphi_s(n) \quad (3)$$

$$Q \propto E_{\mathrm{L}}(n)E_{\mathrm{R}}(n)\sin\varphi_s(n). \quad (4)$$

Then the phase information and amplitude of $S(n)$ can be obtained by the following two formulas:

$$E(n) = \sqrt{I^2 + Q^2} \quad (5)$$

$$\varphi_s(n) = \arctan\left(\frac{Q}{I}\right). \quad (6)$$

When sensing optical fiber external disturbance, the disturbance position of the backward Rayleigh scattering optical phase changes, causing the corresponding position
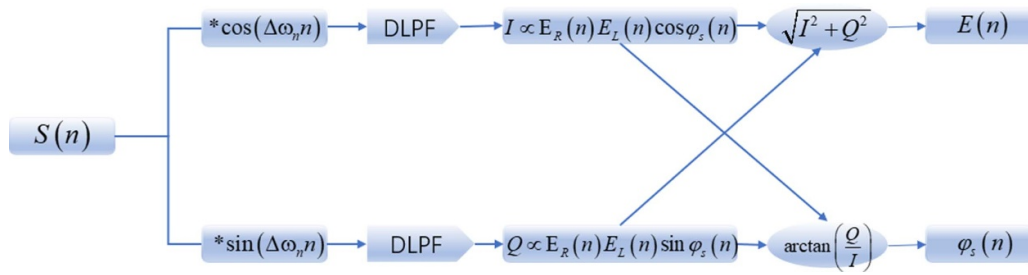
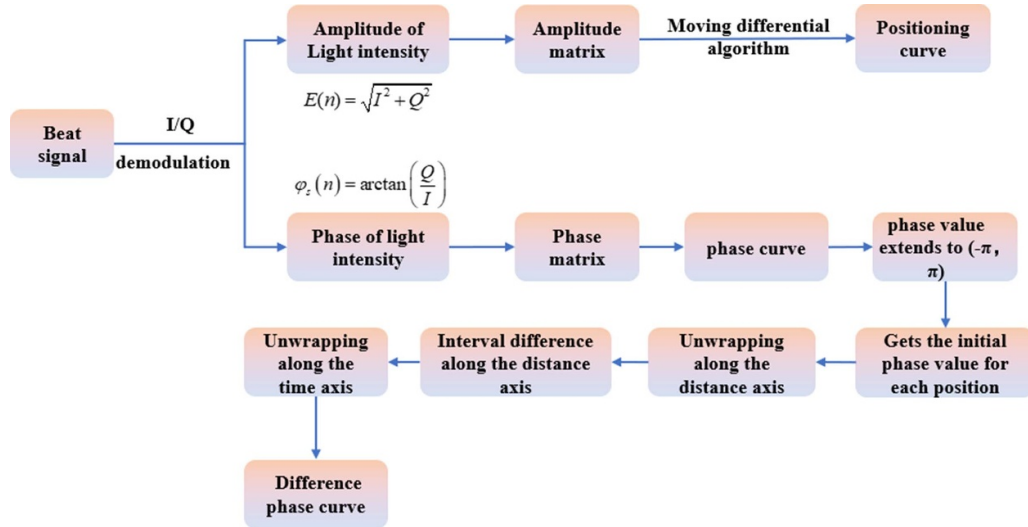**Figure 3.** Digital I/Q demodulation algorithm.

Figure 4. Signal processing flowchart.

of the Rayleigh scattering light amplitude to change, so by demodulating the amplitude change of $S(n)$ we can fix the position of disturbance; from the change of $\varphi_s(n)$, we can find the intensity and frequency of disturbance. Since the value of $\varphi_s(n)$ is obtained by the inverse tangent operation, the phase information is wrapped in the range of $(-\pi/2, +\pi/2)$. In order to obtain the real phase change information, the range can be extended to $(-\pi, +\pi)$ first, and the phase value can be expanded by the phase unwrapping algorithm [24]. Because phase wrapping exists in the phase difference of both the distance domain and the time domain, secondary unwrapping is required. Finally, the curve of the phase difference information of the disturbed position with time can be obtained. The complete processing flow of the system signal is shown in figure 4.

3. Results and discussion

3.1. Single frequency disturbance detection

In this part, by demodulating the beat signal with the I/Q demodulation algorithm, both the phase and amplitude of the disturbance signal are obtained. The full length of the FUT used is 6 km, and using PZT wrapped in 10 m fiber to simulate the sinusoidal disturbance signal at about 4.96 km, the frequency of this disturbance signal is 50 Hz and the amplitude is 1.5 V (peak-to-peak value). Afterward, in order to verify the

restoration performance of the system for different kinds of signals, a triangular wave disturbance signal with an amplitude of 3 V and a frequency of 50 Hz is used to interfere with the fiber at the same location. Figure 5 shows the detected position of the applied sinusoidal and triangular wave disturbance signals by the system. The moving difference algorithm [25] is used to locate the disturbance. The measured spatial resolution is 10.7 m, which corresponds to a theoretical spatial resolution of 10 m.

Figure 6(a) gives the phase change of the fiber at 4.96 km. It can be seen that no phase change can be observed in the unperturbed area, while in the perturbed area, the phase change exhibits regularity in the form of a sine wave. Figure 6(b) shows the phase information applied to triangular wave signals at the same position; the phase change of the disturbance region is obvious and periodic. In the vibration field of the fiber, it is obvious that the period in which the phase information changes with time is 0.02 s; this corresponds exactly to a 50 Hz perturbation signal generated by the piezoelectric ceramic.

3.2. Superposition signal recovery and decomposition and linear response

Two sinusoidal signals with the same amplitude are mixed and superimposed; their frequencies are 150 Hz and 100 Hz, so
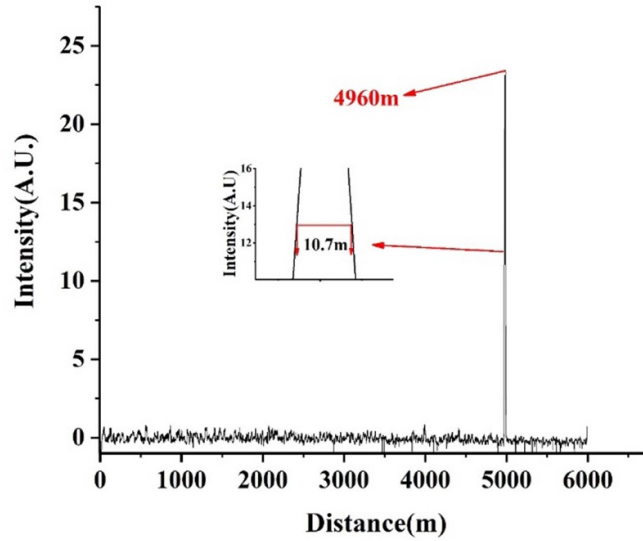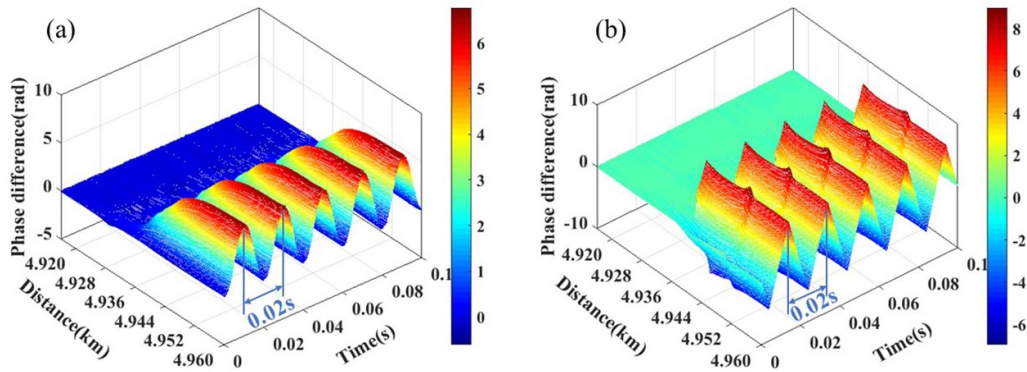
Figure 5. Perturbation location map.

Figure 6. Spatiotemporal diagram of disturbance position: (a) sinusoidal vibration signal phase information at 4.96 km, (b) triangular wave vibration signal phase information.

that a multi-frequency superposition signal is obtained. The superimposed signal is generated by an AWG and transmitted to the piezoelectric ceramic as a driving signal. As shown in figure 7(a), using the I/Q demodulation algorithm combined with a secondary unwrapping algorithm to obtain the phase value of the disturbance, the curve of restored phase difference versus time shows that the restoration effect is very significant and basically without distortion. Figure 7(b) shows the spectrum of the superimposed signal; obviously, the frequencies of the superposition signal are composed of 100.10 Hz and 150.15 Hz, which agrees well with the actual applied signal. At the same time, it can be inferred from the power spectrum density map in figure 7(c) that the SNR of the recovered mixed-frequency signal can reach 45.84 dB, which reflects the excellent detection performance of the system.

Figure 8(a) plots the spatiotemporal diagram of disturbance position, where the colors indicate the magnitude of the phase difference obtained after demodulation; it is obvious that the color of the disturbance area at 4.96 km changes regularly with time. Next, we attempt to decompose the superposition signal

through a finite impulse response (FIR) filter. As shown in figure 8(b), a 100 Hz sinusoidal signal and a 150 Hz sinusoidal signal can be obtained, and more importantly, they have the same amplitude, which is consistent with the disturbance signal imposed by PZT.

In order to test the linearity of the system in restoring signals of different amplitudes, the amplitudes of two sinusoids with different frequencies are changed at the same time. First, the 150 Hz sinusoidal signal (1.5 V) and the 100 Hz sinusoidal signal (13.5 V) are mixed and superimposed, and then the amplitude of the 150 Hz sinusoidal signal is increased with a step value of 1.5 V while that of the 100 Hz sinusoidal wave is reduced with a step value of -1.5 V. As shown in figure 9, when the driving voltage of PZT is changed, the signal amplitude obtained after restoration increases or decreases correspondingly, and the linearity is very good. It can be seen that the linear fitting between the change of sinusoidal wave amplitude at 150 Hz and the driving voltage of PZT is $R^2 = 0.9997$, and the linear fitting between the change of sinusoidal wave amplitude and the driving voltage of PZT at
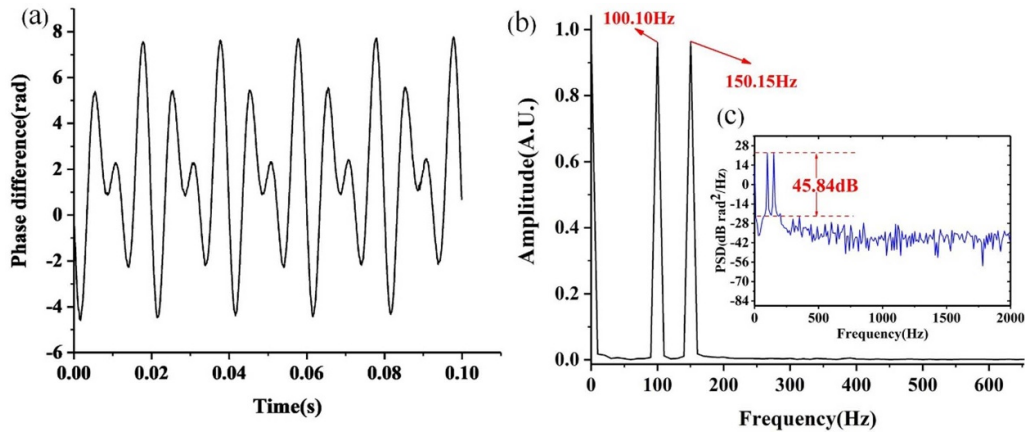
Figure 7. (a) Restored phase difference–time curve, (b) spectrum of the signal, (c) corresponding power spectrum density (PSD) map.
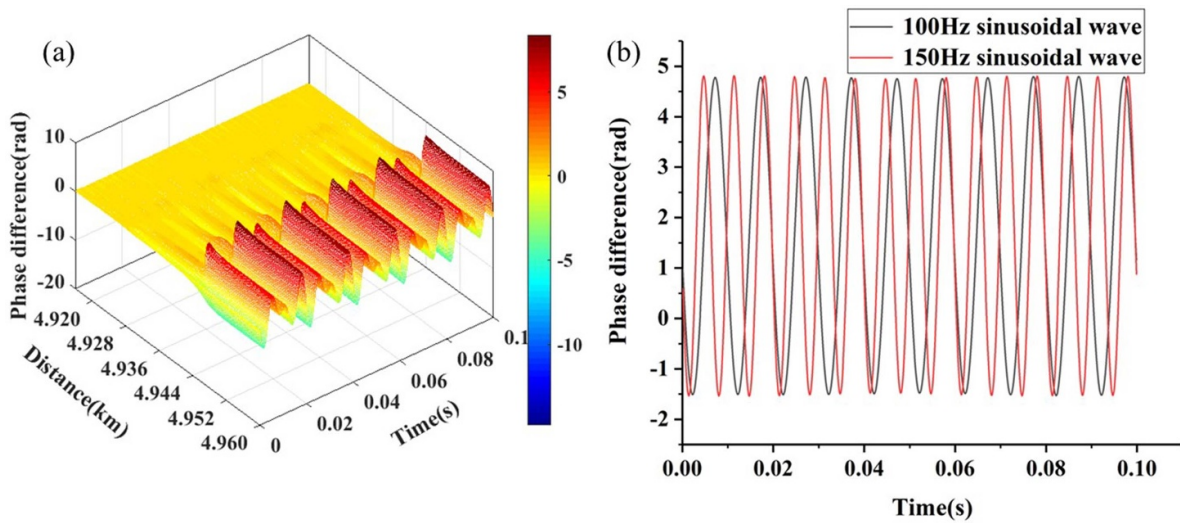

Figure 8. (a) Spatiotemporal diagram of disturbance position, (b) phase difference–time diagram of two signals obtained after decomposition.

100 Hz is $R^2 = 0.9998$. Obviously, the system has a very high linear response, which can retain the details of each frequency component of the superimposed signal well without signal loss. Therefore, even if the amplitude of each frequency component in the superposition signal changes, the system can recover them well.

In the previous experiment, two signals of the same type are mixed and superimposed. It can be seen that the recovery effect is very good, so if two different types of signal are mixed, can it have the same effect? To verify the question, a sinusoidal wave and triangular wave of the same amplitude are mixed and superimposed, in which the frequency of the triangular wave is 150 Hz and the frequency of the sine wave is 50 Hz, so as to obtain a superimposed signal. Again, this superimposed signal is output to PZT as a drive signal through the function generator. Figure 10(a) is the curve of phase difference versus time obtained after restoration. It can be seen that the restoration effect is very significant and basically without distortion as before. The spectrogram of this mixed signal is shown in figure 10(b); it is obvious that the frequency of this signal is exactly composed of 150.15 Hz and 50.05 Hz.

Figure 11(a) plots the time–space image of the phase values after demodulation; regular changes can be seen in the disturbed region, which is consistent with the disturbance signal imposed by PZT. Similarly, we separate the two signals through an FIR filter. As shown in figure 11(b), two signals of the same amplitude can be obtained: one is a 150 Hz triangular wave and the other is a 50 Hz sinusoidal wave. Obviously, this corresponds to the signal applied to PZT in practice.

Next, in order to verify the linearity of the system in restoring signals of different amplitudes and types, we change the amplitudes of the two signals at the same time. First, the 150 Hz triangular signal (1.5 V) and the 50 Hz sinusoidal signal (13.5 V) are superimposed, and then the 150 Hz triangular wave is increased with a step value of 1.5 V. The 50 Hz sinusoidal wave decreases with a step value of −1.5 V. It can be seen from figure 12 that the fitting linearity of the two signals is very good. The fitting coefficient of the restored
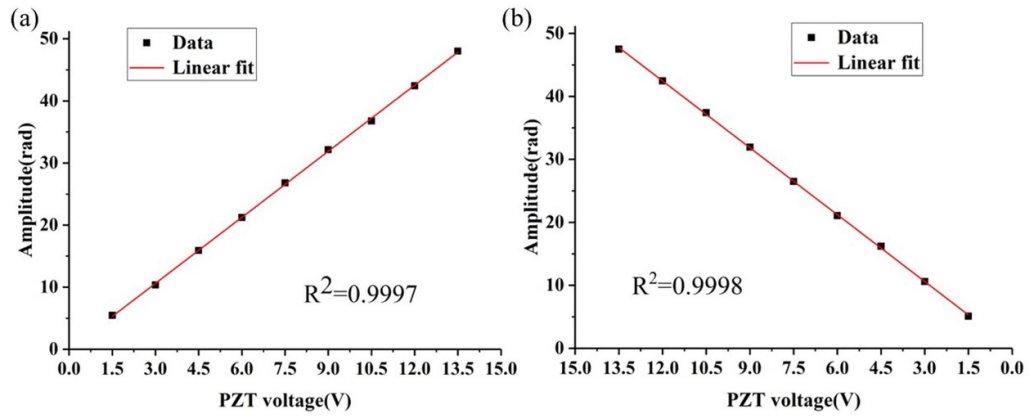
Figure 9. Curve of demodulation signal phase amplitude changing with PZT driving voltage: (a) 150 Hz sinusoidal signal, (b) 100 Hz sinusoidal signal.
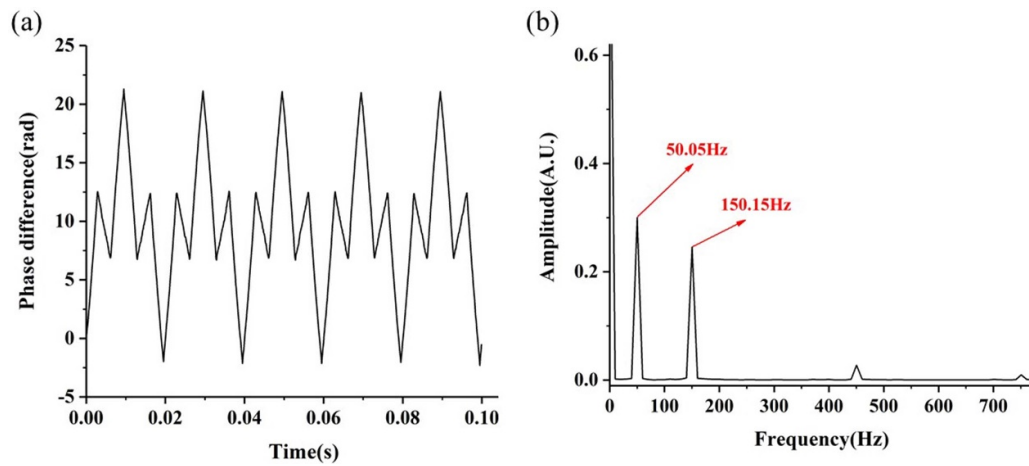

Figure 10. (a) Restored phase difference–time curve, (b) spectrum of the signal.
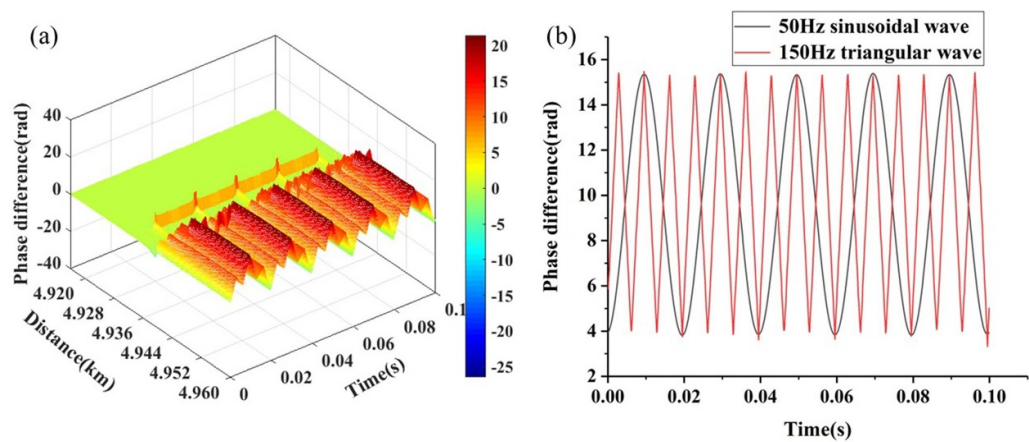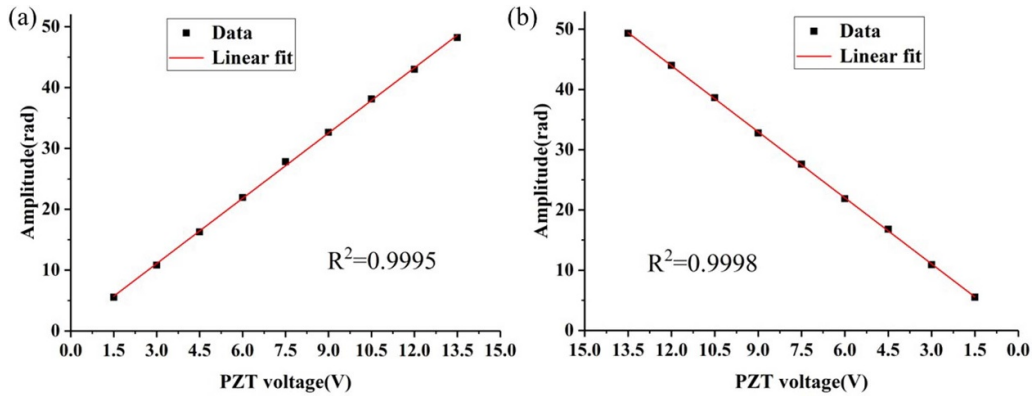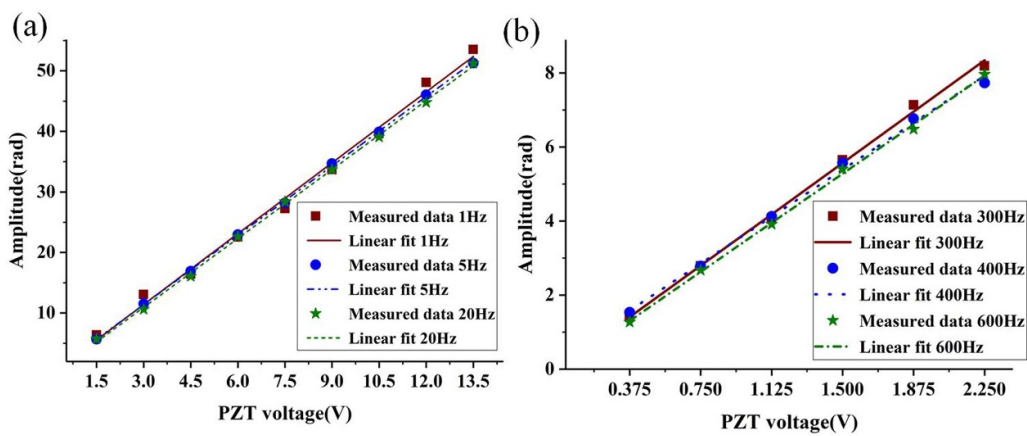

Figure 11. (a) Spatiotemporal diagram of disturbance position, (b) phase difference–time diagram of two signals obtained after decomposition.

Figure 12. Curve of demodulation signal phase amplitude changing with PZT driving voltage: (a) 150 Hz triangle signal, (b) 50 Hz sinusoid signal.

Figure 13. Curve of demodulation signal phase amplitude changing with PZT driving voltage: (a) when vibration frequency is 1 Hz (red), 5 Hz (blue) and 20 Hz (green), (b) when vibration frequency is 300 Hz (red), 400 Hz (blue) and 600 Hz (green).

triangular wave amplitude and the driving voltage applied by PZT is $R^2 = 0.9995$, and the fitting coefficient of the restored sinusoidal wave amplitude and the driving voltage applied by PZT is $R^2 = 0.9998$.

Because the common disturbance behavior is usually in the low frequency signal, the linear responsiveness of the system to the lower frequency signal is very important. Therefore, three experiments with vibration frequencies of 1 Hz, 5 Hz and 20 Hz are conducted. The voltage applied in each experiment varies from 1.5 V to 13.5 V with a step change of 1.5 V. Figure 13(a) shows a linear fit between the phase difference information and the applied voltage. The R^2 values for the 1 Hz, 5 Hz and 20 Hz linear fitting results are 0.9935, 0.9997 and 0.9993 respectively. In order to further verify the linear response of the system in higher frequency signals, an additional three vibration frequencies of 300 Hz, 400 Hz and 600 Hz are applied to the sensor. In the experiment, the voltage changes from 0.375 V to 2.25 V with a step change of 0.375. Figure 13(b) shows a linear fit between the phase difference and the applied voltage. The linear fitting R^2 values for 300 Hz, 400 Hz and 600 Hz are 0.9978, 0.9968 and 0.9988 respectively, indicating a good linear response of the system at higher

frequencies. Comparison results with similar phase extraction techniques are shown in table 1.

3.3. Recovery of harmonic signal and sweep signal

Moreover, a four harmonic signal is verified by the system. The four harmonic signal with a harmonic frequency of 25 Hz is applied by the PZT at 4.96 km of the FUT. Figure 14(a) shows the curve of phase difference with time obtained by demodulation, and it can be seen that the restored signal basically has no distortion. Figure 14(b) shows the spectrum diagram of the harmonic signal; the peak values of frequency are 25.012 Hz, 50.025 Hz, 75.037 Hz and 100.05 Hz. This further proves that the harmonic signal is successfully recovered.

Next, in order to verify the signal recovery ability of the system to dynamic frequency changes, we use a function generator to output a sinusoidal sweep signal (from 50 Hz up to 250 Hz and then down to 50 Hz) to PZT. The result is as shown in figure 15(a). After restoration, a sweep curve of phase difference with time can be obtained. Then the short-time Fourier transform algorithm is used to obtain the time–frequency diagram of the scanning signal. It can be seen from figure 15(b)

Table 1. Comparison of demodulation results with similar techniques.

Structure	Demodulation method	Performance	Year	References
Homodyne coherent detection	I/Q demodulation	SNR: 34.1 dB Spatial resolution: 10 m Linear fitting: $R^2 = 0.9740$	2016	[19]
Direct detection	Improved PGC demodulation	SNR: 30.34 dB Spatial resolution: 10 m Sensing distance: 2 km	2018	[20]
Michelson interferometer (MI) based on 3×3 coupler	Ellipse fitting differential cross multiplication (EF-DCM)	SNR: 57.9 dB Frequency range: 0.8 Hz–250 Hz Linear fitting: 0.9980	2020	[21]
Direct detection	Phase-shifted dual-pulse probes	SNR: 35 dB Sensing distance: 5 km Frequency range: 0.5 Hz–20 Hz Linear fitting: $R^2 = 0.9987$	2022	[22]
Heterodyne coherent detection	Digital I/Q demodulation algorithm	SNR: 45.84 dB Frequency range: 1 Hz–600 Hz Sensing distance: 7 km Linear fitting: $R^2 = 0.9997$	2022	This paper
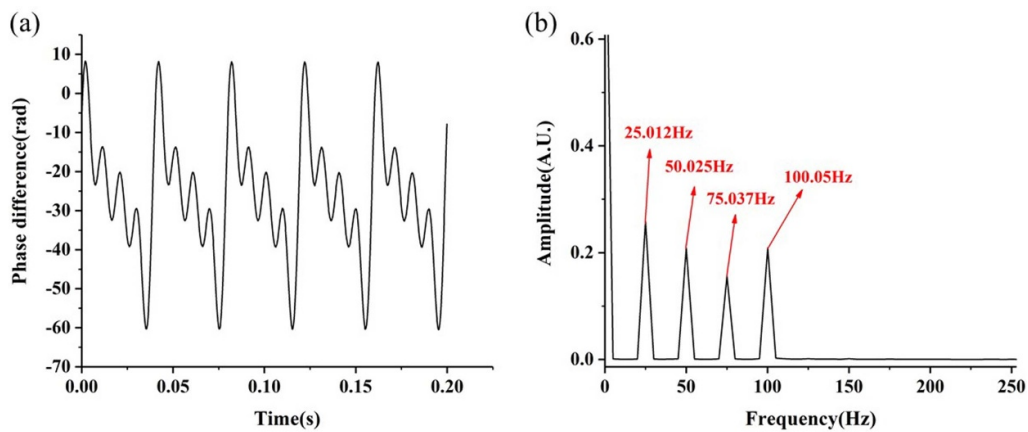
Figure 14. (a) Phase difference curve with time of the recovered fourth harmonic signal, (b) spectrum of the signal.
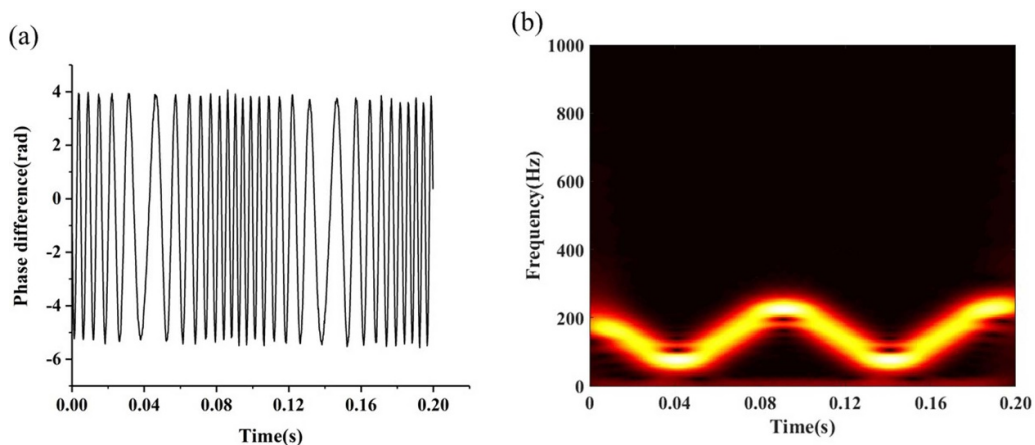
Figure 15. (a) Phase difference curve with time of the restored sweep signal, (b) time–frequency diagram of a sweep signal.
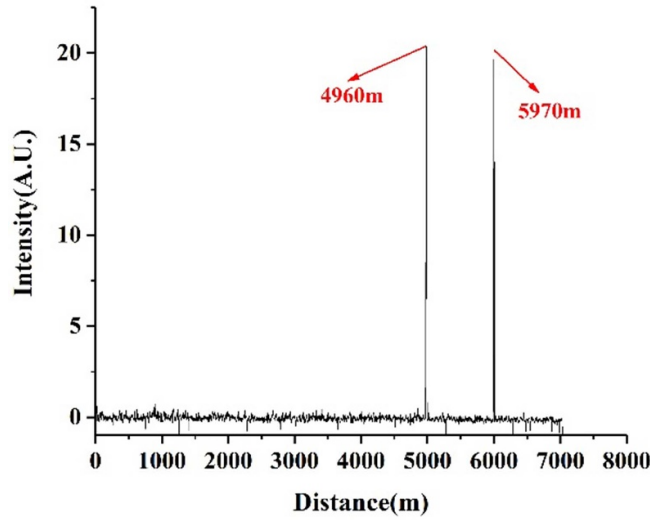
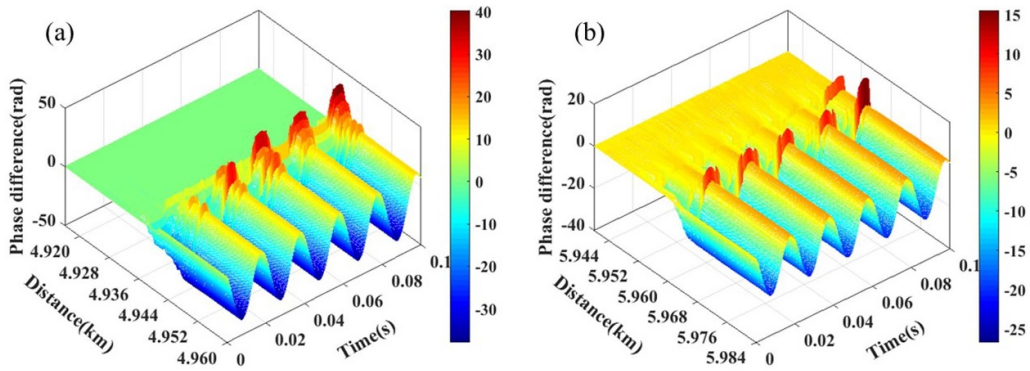**Figure 16.** Location diagram of two points of disturbance.

Figure 17. Spatiotemporal diagram of disturbance position: (a) disturbance area at 4.96 km, (b) disturbance area at 5.97 km.

that the frequency change of the sweep signal conforms to the actual situation with the transformation of time.

3.4. Detection of two simultaneous disturbances

Generally, in a practical situation, disturbances may occur in more than one place, so whether the system has the ability of multi-point detection is also important. In order to detect the simultaneous monitoring of multi-point disturbance signals by the system, using PZT, 50 Hz sinusoidal disturbance signals are simultaneously applied at 4.96 km and 5.97 km of an optical fiber with a total length of 7 km. Figure 16 is the disturbance location diagram obtained by the moving difference algorithm. Two peaks are clearly visible at the locations of the disturbances.

Figure 17 shows the spatiotemporal diagrams of the disturbed area. Regular sinusoidal disturbances can be seen in the disturbed area. Therefore, the system also has good performance in multi-point detection. This is also more consistent with the actual application scenario.

3.5. Characterization parameters

In order to further verify the repeatability and error analysis of the system, four different types of disturbance signals were determined, and experimental tests were repeated six times. Figures 18(a) and (b) show the measured amplitudes and error bars of these tests. Obviously, the error in each disturbance frequency experiment is very small and has very good repeatability.

The length of the fiber wound on the PZT is about 10 m, and the fiber tensile coefficient is 0.4 μm V^{-1}. Assuming the signal has a frequency of 20 Hz, when the PZT is applied to 6 V voltage, the calculated acoustic induced strain is 240 nε and the recovered phase difference amplitude is 22.61 rad. Therefore, the strain sensitivity of the system is $240/22.61 = 0.09$ rad nε^{-1}. In the process of our measurement, the magnitude of phase fluctuation generated by the system is 0.21 rad without any disturbance, so the calculated strain resolution of the system is 2.33 nε. It is noted that Rayleigh scattering is not sensitive to temperature variation; the φ-OTDR in this paper is temperature insensitive.
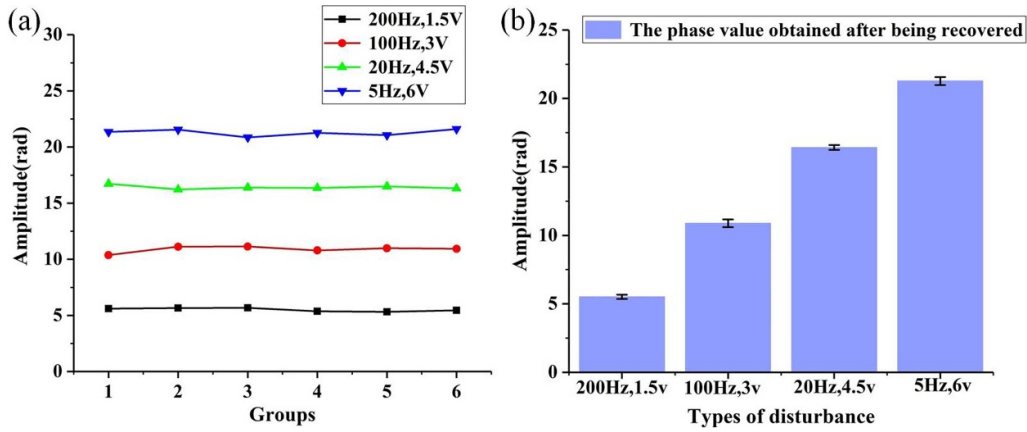
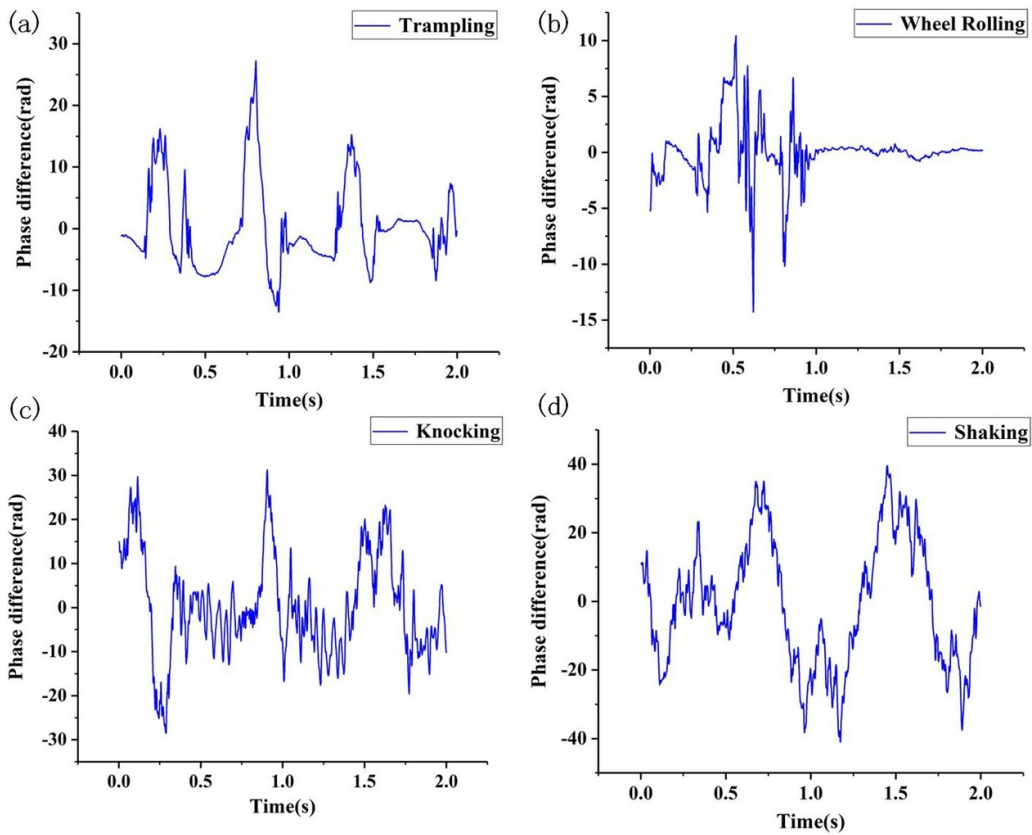**Figure 18.** (a) Repeatability test, (b) error analysis.

Figure 19. Four kinds of disturbance signals: (a) trampling, (b) wheel rolling, (c) knocking, (d) shaking.

3.6. Quick field validation tests

In order to verify the actual on-site detection capability, we build two scenarios: hanging net type and floor type. In addition, we apply two perturbation modes in the two scenarios, in which the perturbation modes of knocking and shaking are applied in the hanging net type, and human trampling and wheel rolling are used in the floor type. In order to better compare the differences between different disturbance signals, the disturbance acquisition time is unified as 2 s.

Figure 19 shows the four disturbance signals recovered from the on-site detection, which are human trampling, wheel rolling, knocking, and shaking. The results show that different perturbation modes have obvious differences in amplitude and waveform. This lays a good foundation for follow-up research on the application of pattern recognition in perimeter security.

4. Conclusion

In this paper, a φ-OTDR system based on heterodyne coherent detection is built, which can recover the real phase information of external disturbances very effectively in quantitative detection of multi-frequency disturbances. Not only the

11

superposition signal composed of two sinusoidal waves of different frequencies but also that composed of two different frequencies and different kinds of signals are recovered. More importantly, by using the fast Fourier transform to get the frequency of the superimposed signal, combined with the use of FIR filter, the superposed signal is decomposed according to its frequency components, perfectly restoring the two signals before they are superimposed, and their amplitude is highly linear with the driving voltage of the PZT. Furthermore, in the experiment of harmonic signal and sweep disturbance signal, the system has good detection ability and no distortion. The above shows that the system can retain the details of each frequency component well in the recovery of multi-frequency signals. In addition, the system can also detect multi-point simultaneous disturbance signals. In this article, the most important finding is a quantitative detection of the external multi-frequency disturbance signal, rather than just being restricted to single-frequency experiments, more in line with actual application scenarios. At the same time, four different disturbance signals (human trampling, wheel rolling, knocking, and shaking) are recovered by rapid field verification. The system has excellent detection performance and has broad application prospects in the field of perimeter security, especially to establish a good foundation for identifying different kinds of intrusion behavior experiments.

Data availability statement

No new data were created or analyzed in this study.

Acknowledgments

ORCID iDs

Bin Liu ⬤ https://orcid.org/0000-0002-7971-3841
Qiang Wu ⬤ https://orcid.org/0000-0002-2901-7434

References

[1] Pang F F, He M T, Liu H H, Mei X W, Tao J M, Zhang T Z, Zhang X B, Chen N and Wang T Y 2016 A fading-discrimination method for distributed vibration sensor using coherent detection of φ-OTDR *IEEE Photonics Technol. Lett.* **28** 2752–5

[2] Liu Z, Zhang L, Wei H, Xiao Z, Qiu Z, Sun R, Pang F and Wang T 2021 Underwater acoustic source localization based on phase-sensitive optical time domain reflectometry *Opt. Express* **29** 12880–92

[3] Dorize C, Awwad E and Renaudier J 2019 High sensitivity φ-OTDR over long distance with polarization multiplexed codes *IEEE Photonics Technol. Lett.* **31** 1654–7

[4] Min R, Liu Z, Pereira L, Yang C, Sui Q and Marques C 2021 Optical fiber sensing for marine environment and marine structural health monitoring: a review *Opt. Laser Technol.* **140** 107082

[5] Peng F, Duan N, Rao Y J and Li J 2014 Real-time position and speed monitoring of trains using phase-sensitive OTDR *IEEE Photonics Technol. Lett.* **26** 2055–7

[6] Wang F, Liu Z, Zhou X, Li S, Yuan X, Zhang Y, Shao L and Zhang X 2021 Oil and gas pipeline leakage recognition based on distributed vibration and temperature information fusion *Results Opt.* **5** 100131

[7] Ruiz A G, Lopez A D, Graells J P, Martins H F, Lopez S M and Herraez M G 2018 Long-range distributed optical fiber hot-wire anemometer based on chirped-pulse φ-OTDR *Opt. Express* **26** 463–76

[8] Chen W, Ma X H, Ma Q L and Wei J J 2021 Denoising method of the φ-OTDR system based on EMD-PCC *IEEE Sens. J.* **21** 12113–8

[9] Peng F, Wu H, Jia X H, Rao Y J, Wang Z N and Peng Z P 2014 Ultra-long high-sensitivity φ-OTDR for high spatial resolution intrusion detection of pipelines *Opt. Express* **22** 13804–10

[10] Zhu T, Xiao X H, He Q and Diao D M 2013 Enhancement of SNR and spatial resolution in φ-OTDR system by using two-dimensional edge detection method *J. Lightwave Technol.* **31** 2851–6

[11] Lu B, Pan Z Q, Wang Z Y, Zheng H R, Ye Q, Qu R H and Cai H W 2017 High spatial resolution phase-sensitive optical time domain reflectometer with a frequency-swept pulse *Opt. Lett.* **42** 391–4

[12] Lyu C G, Jiang J Y, Li B H, Huo Z H and Yang J C 2021 Abnormal events detection based on RP and inception network using distributed optical fiber perimeter system *Opt. Lasers Eng.* **137** 106377

[13] Juarez J C and Taylor H F 2005 Polarization discrimination in a phase-sensitive optical time-domain reflectometer intrusion-sensor system *Opt. Lett.* **30** 3284–6

[14] Zhou J, Pan Z, Ye Q, Cai H, Qu R and Fang Z 2013 Characteristics and explanations of interference fading of φ-OTDR with a multi-frequency source *J. Lightwave Technol.* **31** 2947–54

[15] Wang C, Wang C, Shang Y, Liu X H and Peng G D 2015 Distributed acoustic mapping based on interferometry of phase optical time-domain reflectometry *Opt. Commun.* **346** 172–7

[16] Masoudi A and Newson T P 2017 High spatial resolution distributed optical fiber dynamic strain sensor with enhanced frequency and strain resolution *Opt. Lett.* **42** 290–3

[17] Fang G S, Xu T W, Feng S W and Li F 2015 Phase-sensitive optical time domain reflectometer based on phase-generated carrier algorithm *J. Lightwave Technol.* **33** 2811–6

[18] Shang Y, Yang Y H, Wang C, Hui L X, Wang C and Pang G D 2016 Optical fiber distributed acoustic sensing based on the self-interference of Rayleigh backscattering *Measurement* **79** 222–7

[19] Wang Z N, Zhang L, Wang S, Xue N T, Peng F, Fan M Q, Sun W, Qian X Y, Rao J R and Rao Y J 2016 Coherent φ-OTDR based on I/Q demodulation and homodyne detection *Opt. Express* **24** 853–8

[20] Yu Z H, Zhang Q, Zhang M Y, Dai H L, Zhang J J, Liu L, Zhang L J, Jin X, Wang G F and Qi G 2018 Distributed optical fiber vibration sensing using phase generated carrier demodulation algorithm *Appl. Phys.* B **124** 84

[21] Fang P J, Yan W, Lu P, Zhang W J, Zhang W, Fu X and Zhang J S 2020 High sensitivity fiber-optic Michelson interferometric low-frequency acoustic sensor based on a gold diaphragm *Opt. Express* **28** 25238–49

[22] Liu S Q *et al* 2022 Quantitative demodulation of distributed low-frequency vibration based on phase-shifted dual-pulse phase-sensitive OTDR with direct detection *Opt. Express* **30** 10096–109

[23] Wang P F, Xu N, Wang Y, Liu X, Gao Y, Jin B Q and Zhang H J 2022 Multiresolution phase compensation for phase-sensitive OTDR *IEEE Sens. J.* **22** 14937–43

[24] Zhu F, Zhang Y X, Xia L, Wu X L and Zhang X P 2015 Improved φ-OTDR sensing system for high-precision dynamic strain measurement based on ultra-weak fiber Bragg grating array *J. Lightwave Technol.* **33** 4775–80

[25] Lu Y L, Zhu T, Chen L and Bao X Y 2010 Distributed vibration sensor based on coherent detection of phase-OTDR *J. Lightwave Technol.* **28** 3243–9